| Title | Anomalously Low Heat Conduction in Single-Crystal Superlattice Ceramics Lower Than Randomly Oriented Polycrystals |
|---|---|
| Author(s) | Cho, Hai Jun; Wu, Yuzhang; Zhang, Yu-Qiao; Feng, Bin; Mikami, Masashi; Shin, Woosuck; Ikuhara, Yuichi; Sheu, Yu-Miin; Saito, Keiji; Ohta, Hiromichi |
| Citation | Advanced Materials Interfaces, 8(7), 2001932. https://doi.org/10.1002/admi.202001932 |
| Issue Date | 2021-04-09 |
| Doc URL | http://hdl.handle.net/2115/84751 |
| Rights | This is the peer reviewed version of the following article: Cho, H. J., Wu, Y., Zhang, Y. Q., Feng, B., Mikami, M., Shin, W., Ikuhara, Y., Sheu, Y. M., Saito, K., Ohta, H., Anomalously Low Heat Conduction in Single Crystal Superlattice Ceramics Lower Than Randomly Oriented Polycrystals. Adv. Mater. Interfaces 2021, 8, 2001932, which has been published in final form at https://doi.org/10.1002/admi.202001932. This article may be used for non-commercial purposes in accordance with Wiley Terms and Conditions for Use of Self-Archived Versions |
| Type | article (author version) |
| File Information | Revised manuscript.pdf |

# Anomalously Low Heat Conduction in Single-Crystal Superlattice Ceramics Lower than Randomly Oriented Polycrystals

*Hai Jun Cho\*, Yuzhang Wu, Yu-qiao Zhang, Bin Feng, Masashi Mikami, Woosuck Shin, Yuichi Ikuhara, Yu-Miin Sheu, Keiji Saito, and Hiromichi Ohta\**

Prof. H.J. Cho, Dr. Y. Zhang, Prof. H. Ohta
Research Institute for Electronic Science, Hokkaido University, N20W10, Kita, Sapporo 001-0020, Japan
E-mail: joon@es.hokudai.ac.jp, hiromichi.ohta@es.hokudai.ac.jp

Prof. H.J. Cho, Y. Wu, Prof. H. Ohta
Graduate School of Information Science and Technology, Hokkaido University, N14W9, Kita, Sapporo 060−0814, Japan

Prof. B. Feng, Prof. Y. Ikuhara
Institute of Engineering Innovation, The University of Tokyo, 2-11-16 Yayoi, Bunkyo, Tokyo 113-8656, Japan

Dr. M. Mikami, Dr. W. Shin
Inorganic Functional Materials Research Institute, National Institute of Advanced Industrial Science and Technology (AIST-Chubu), Anagahora 2266-98, Shimoshidami, Moriyama, Nagoya 463-8560, Japan

Prof. Y.-M. Sheu
Center for Emergent Functional Matter Science, National Chiao Tung University, Hsinchu, 30010, Taiwan

Prof. K. Saito
Department of Physics, Keio University, 3-14-1 Hiyoshi, Kohoku-ku, Yokohama 223-8522, Japan

**Heat conduction in ceramics is attributed to phonon propagation, which can be strongly suppressed at boundaries. Usually, polycrystals show lower thermal conductivity ($\kappa$) than single crystals, as polycrystals contain many grain boundaries. For functional applications in thermal management technologies, ceramics with low thermal conductivity are required. While grain boundary engineering is effective for reducing $\kappa$, its utilization is limited by the fact that other functional properties are often damaged. Here we show that single-crystalline oxide of $InGaO_3(ZnO)_m$ with a natural superlattice structure exhibits anomalously lower $\kappa$ than polycrystals. We fabricated single-**

**crystalline films of $InGaO_3(ZnO)_m$ ($m$ = integer), which has a superlattice structure of $InO_2^-/GaO(ZnO)_m^+$ stacking along the $c$-axis with a controllable layer thickness of $m$. We found the $\kappa$ perpendicular to the superlattices decreased with decreasing $m$-value, and the minimum $\kappa$ was 1.1 W m$^{-1}$ K$^{-1}$ ($m$ = 4, 5), which is lower than randomly-oriented polycrystalline $InGaO_3(ZnO)_m$. On the other hand, the $\kappa$ parallel to the superlattices were similar values with those of polycrystalline. The present finding suggests that layer boundaries between different components inside single-crystal could also function as thermal resistance, which would be useful for the material design of thermal management technologies.**

Understanding the conduction of heat in ceramics is an essential requirement in functional applications in thermal management technologies such as thermoelectrics[1, 2] and thermal barrier coatings[3-6]. The ability for a given material to sustain a flow of heat is quantified with the thermal conductivity ($\kappa$), which is mainly attributed to phonon propagation in case of ceramic materials. Since phonon propagation is greatly hindered at crystalline defects including impurity, vacancies, and boundaries, the $\kappa$ of polycrystalline ceramic materials monotonically decreases with decreasing grain size due to the presence of grain boundaries, where the thermal transport property is quantified with the ratio between the heat flux and temperature discontinuity, known as Kapitza resistance ($R_K$)[7, 8]. For this reason, intrinsic single crystal $\kappa$ is always considered as an upper bound for the heat transport properties of a given material system. Although controlling the grain size is an effective way to tailor the $\kappa$, grain boundaries substantially reduce other important functional properties like electrical conductivity. Therefore, it is important to search materials with low $\kappa$ in the single-crystalline form.

In this regard, the $\kappa$ of layered structures has attracted significant attention, as they exhibit boundaries even in single crystalline forms, which can act as thermal barriers. One example is the derivative of perovskite structures, such as Ruddlesden-Popper and Aurivillus phases. Anisotropy is expected from the $\kappa$ of these structures, which was investigated by comparing polycrystalline materials with randomly oriented grains and those with high orientation index along perpendicular to the layers. The $\kappa$ values observed from the textured specimen were ~1 W m$^{-1}$ K$^{-1}$ perpendicular to the layers and ~2 W m$^{-1}$ K$^{-1}$ parallel to the layers, whereas the $\kappa$ of randomly oriented specimens were in between the two values (along the two directions)[9, 10]. These values are close to amorphous materials[11] as well as theoretical minimum $\kappa$ values[12, 13], which confirm that inter-layer interface in layered structures effectively hinder the propagation of heat. In fact, the lowest $\kappa$ value in a solid was observed from a layered structure, known as the turbostratic disorder. This material system consists of disordered layered basal plane crystals and exhibits $\kappa$ values less than 0.1 W m$^{-1}$ K$^{-1}$, which is attributed to strongly localized lattice vibrations[14-18]. There were also computational efforts with *ab-initio* calculations to quantify the heat conduction across the interfaces, and the results indicated that the boundary conductance enhances with increasing interface density[19].

Clarifying the anisotropy and the role of interfaces are the key in understanding the heat conduction in the layered structures. However, most of the studies so far were performed using polycrystalline. In single-crystalline layered materials, the boundaries between the layers are periodic along a certain direction, and there is only one $R_K$ associated with the flow of heat. However, in polycrystalline, the flow of heat is affected by two different $R_K$ values associated with the intra-layer boundaries (parallel to basal planes) and grain boundaries. Furthermore, if the grains are randomly oriented (**Fig. 1a**), the anisotropic heat conduction may also affect the resultant interpretation of $R_K$. Therefore, although the conduction of heat in ceramics with layered structures behavior has been widely studied, there has been no study

that clarifies the anisotropic $\kappa$ and the role of intra-layer Kapitza resistance in the heat conduction of layered structures.

Layered structures/superlattices are mostly synthesized in forms of bulk polycrystalline materials[20-23]. However, correctly identifying the anisotropy and the effect of $R_k$ in a layered material system requires comparing the given material in single crystalline forms in different orientations. Single crystalline layered structure/superlattices are mostly fabricated in forms of thin epitaxial films[24], but in this approach, the crystallographic orientation is extremely difficult to control, as the layers tend to grow perpendicular to the growth direction. In addition, the periodicity of the layered structure should be controllable to correctly analyze the $R_K$. Therefore, the major challenge in addressing the fundamental heat conduction in layered structure has been finding the right layered material system.

In this study, to investigate the intrinsic $\kappa$ in single-crystalline layered materials, we focus on the homologous phases of $InGaO_3(ZnO)_m$ ($m$ = integer), which is composed of atomically thin $InO_2^-$ layers and $GaO_3(ZnO)_m^+$ blocks alternately stacked along the $c$-axis.[20-23] This crystal structure is a superlattice of $InO_2^-/GaO_3(ZnO)_m^+$, and the superlattice period ($d_{SL}$) changes from ~0.87 nm (monolayer $GaO_3(ZnO)_m^+$) to infinity as the $m$-value increases. Thus, the interface density can be controlled in this material system[25], and the $R_K$ can be clarified by modulating the $m$-value. They can naturally occur at high temperature and mimic the orientation of the substrate[25], enabling the orientation control. Furthermore, this material can also be synthesized in bulk polycrystalline form, and the $\kappa$ of single-crystalline films and polycrystalline can be compared directly as schematically shown in **Figs. 1a and 1b**. Several studies attempted to examine the thermal transport properties of this material system. However, they were limited by the use of randomly-oriented polycrystalline or the presence of structural defects like porosities [26-29].

4

Here we clarify the heat conduction in single-crystalline $InGaO_3(ZnO)_m$ superlattice. We fabricated single-crystalline films of $InGaO_3(ZnO)_m$ ($m = 1−35$) in two different orientations on YSZ single-crystalline substrates and measured the thermal conductivity by means of time-domain thermoreflectance (TDTR) method (**Fig. 2**). The superlattice is grown parallel to the substrate surface when (111) YSZ is used, whereas the superlattice is inclined 31.5° from the substrate surface when (110) YSZ is used. Using the former film, we directly measured the thermal conductivity perpendicular to the superlattice ($\kappa_\perp$). The observed $\kappa$ values using the latter film can be decomposed into the $\kappa$ perpendicular to the superlattice ($\kappa_\perp$) and parallel ($\kappa_{//}$) to the superlattice. Thus, we extracted the $\kappa_{//}$ using the following equation[30, 31]:

$$\kappa_{obsd} = \sqrt{\kappa_\perp{}^2 cos^2\theta + \kappa_\parallel{}^2 sin^2\theta}$$

where $\theta$ is 31.5°.

As a result, $\kappa_\perp$ decreased with decreasing $m$-value and the minimum $\kappa$ was 1.1 W m$^{-1}$ K$^{-1}$ ($m$ = 4, 5), which is ~1/3 of the polycrystalline $InGaO_3(ZnO)_m$. On the other hand, $\kappa_{//}$ monotonically decreased until $m = 5$, then plateaued at ~3 W m$^{-1}$ K$^{-1}$. The anomalously low $\kappa$ values perpendicular to the superlattice are attributed to the contribution from $\kappa$ parallel to the superlattice and well-oriented $InO_2{}^-$ layers. The thermal Kapitza resistance at the $InO_2{}^-/GaO(ZnO)_m{}^+$ interface was clarified to be 1.76 m$^2$ K GW$^{-1}$, similar to that of artificial superlattices. The present finding refreshes our understandings towards heat conduction in layered materials, which would be useful for the material design of thermal management technologies.

The $InGaO_3(ZnO)_m$ ($m = 1−35$) single-crystalline films were fabricated by the reactive solid-phase epitaxy (R-SPE) method[25, 32, 33] on (111)- and (110)-oriented yttria-stabilized zirconia

5

(YSZ) single-crystalline substrates. The thicknesses of the resultant InGaO$_3$(ZnO)$_m$ films were 90−250 nm (**Table S1** and **Table S2**). **Figures 3a and 3b** show the X-ray diffraction (XRD) patterns of the InGaO$_3$(ZnO)$_5$ films grown on (a) (111)-oriented YSZ and (b) (110)-oriented YSZ substrates. Intense diffraction peaks of 000$l$ InGaO$_3$(ZnO)$_5$ are seen together with 111 YSZ substrate (*) when the film was grown on (111)-oriented YSZ substrate. On the other hand, intense diffraction peaks of 000l InGaO$_3$(ZnO)$_5$ are seen in the off-axis XRD pattern when the film was grown on (110)-oriented YSZ, indicating that the superlattice was inclined. The incline angle $\theta$ was 31.5°. The peak interval (0.521 nm$^{-1}$) of both samples corresponds to the distance between two adjacent InO$_2^-$ layers (1.92 nm), indicating that the resultant films are single-crystalline InGaO$_3$(ZnO)$_5$. The XRD results for other $m$-values are summarized in **Figures S2 and S3**.

Atomically flat terraced and stepped surfaces were observed in the topographic atomic force microscopy (AFM) image of the InGaO$_3$(ZnO)$_5$ film grown on (111) YSZ substrates (**Fig. 3c**, **Supplementary Fig. S4 a−d**). On the other hand, stripe patterns were observed in the AFM image of the InGaO$_3$(ZnO)$_5$ film grown on (110) YSZ substrates (**Fig. 3d**, **Supplementary Fig. S4 e−h**). These stripe patterns are due to the terraced and stepped surfaces. These observations are consistent with the previous report.

In order to further clarify the superlattice structure, we visualized the atomic arrangement of the InGaO$_3$(ZnO)$_m$ films by using the high-angle annular dark field (HAADF) scanning transmission electron microscopy (STEM). **Figure 4** summarizes the cross-sectional HAADF-STEM image of the InGaO(ZnO)$_{15}$ single-crystalline film grown on (111) YSZ substrate. A superlattice structure composed of InO$_2^-$ layers and GaO(ZnO)$_m^+$ blocks are periodically seen. The heterointerfaces between the Mo transducer film and the top surface of InGaO(ZnO)$_{15}$ film and the (111) YSZ substrate are atomically sharp, suggesting that the

surface/interface roughness does not affect the TDTR measurement. From these results, we confirmed that the excellent crystal quality of $InGaO_3(ZnO)_m$ films for clarifying the anisotropic $\kappa$ and the $R_K$ of $InO_2^-/GaO(ZnO)_m^+$ interfaces.

**Figure 5a** shows the thermal conductivity ($\kappa_\perp$, $\kappa_\parallel$) of the $InGaO_3(ZnO)_m$ superlattices films as a function of the interface density ($d_{SL}^{-1}$). Note that all $InGaO_3(ZnO)_m$ films are electrically insulating, and the heat conduction is solely attributed to the phonon transport. The $\kappa$-values for the random-oriented polycrystalline ceramics of $InGaO_3(ZnO)_m$ are plotted together for comparison. The $\kappa_\perp$ values observed from single-crystalline $InGaO_3(ZnO)_m$ are always lower than all of those observed from bulk polycrystalline superlattices, likely because of the higher $\kappa_\parallel$ values. Despite the presence of grain boundaries, it is surprising to note that the polycrystalline values are close to the $\kappa_\parallel$ values. This seemingly suggests that the heat conduction $InGaO_3(ZnO)_m$ in any orientations is dominated by the in-plane component, but given that the polycrystalline values are highly scattered and from other studies, it is difficult to directly comment on this anomalous behavior. Initially, the $\kappa$ of the single-crystalline $InGaO_3(ZnO)_m$ films monotonically decreases with increasing $d_{SL}^{-1}$ until $d_{SL}^{-1}$ reaches 0.505 $nm^{-1}$ ($d_{SL} = 2.0$ nm). The $\kappa$ then increases when the $d_{SL}^{-1}$ is greater than 0.505 $nm^{-1}$, and the hindrance of heat conduction at the interface is decreasing. Similar trend is also seen in the case of random-oriented polycrystalline ceramics, but the changes in $\kappa$ is not as drastic as those observed from single-crystalline films. The minimum $\kappa$ was 1.1 W $m^{-1}$ $K^{-1}$ ($m = 4, 5$), approximately one third of polycrystalline $InMO_3(ZnO)_m$[34-37]. This surprising result indicates that well-oriented $InO_2^-$ layers in single-crystalline $InGaO_3(ZnO)_m$ superlattice are more effective in reducing the $\kappa$ compared to the case of polycrystalline $InGaO_3(ZnO)_m$. One previous study reported a higher $\kappa$ value for amorphous $InGaZnO_4$ (1.4 W $m^{-1}$ $K^{-1}$)[38], but our own assessment for amorphous $InGaZnO_4$ turned out to be 0.7 W $m^{-1}$ $K^{-1}$[39]. On the

other hand, the $\kappa_\parallel$ values monotonically decrease until $m = 5$, then reach a plateau at ~3 W

$m^{-1}$ $K^{-1}$. This indicated that the dominant phonon scatterings mechanism along the parallel

direction switches from diffuse to specular scattering[40]. Usually, specular scattering is

difficult to experimentally observe along the in-plane direction in superlattices due to the

existence in various defects at interfaces[41-43]. This confirms that the interfaces in our

$InGaO_3(ZnO)_m$ single crystalline films are highly pristine.

We then analyzed the $\kappa_\perp$ results by plotting the thermal resistivity ($R = \kappa_\perp^{-1}$) as a function of

the $d_{SL}^{-1}$ (**Fig. 5b**). Two straight lines A (solid) and B (dotted) could be identified from the

$InGaO_3(ZnO)_m$ single-crystalline films, which intersected at $d_{SL} = 2.0$ nm. When $d_{SL}$ was

longer than 2.0 nm ($m \geq 5$), $R$ increased proportionally with the $d_{SL}^{-1}$. In this regime, the

following equation describes the relationship between $R$ and $d_{SL}$:

$$R = R_0 + R_K \cdot d_{SL}^{-1}$$

where $R_0$ is the $\kappa^{-1}$ of the $GaO(ZnO)_m^+$ block ($m = \infty$). The $R_K$ at $InO_2^-$ layers and the $\kappa$ of

$GaO(ZnO)_m^+$ block ($m = \infty$) were calculated to be 1.76 $\pm0.06$ $m^2$ K $GW^{-1}$ and 20.9 W $m^{-1}$

$K^{-1}$, respectively. Despite being atomically thin, the $R_K$ of $InO_2^-$ layer is much higher than the

$R_K$ of artificially created interfaces between dissimilar materials.[44] This is likely due to the

difference between the atomic mass (Zn, Ga, In) and the effective spring constants of the

atomic bonds, which result in discrepancy in the vibrational density of states between

$GaZnO_2^+$ and $InO_2^-$. This creates discontinuity in the vibrational DOS at the interface, which

causes diffuse scattering. Once the $d_{SL}^{-1}$ exceeds 2.0 nm, $R$ monotonically decreased with

increasing $d_{SL}^{-1}$ ($m < 4$, Line B of **Fig. 5b**). The $R_K$ calculated from the random-oriented

polycrystalline $InGaO_3(ZnO)_m$ ($m \geq 5$) was only 0.46 $m^2$ K $GW^{-1}$, which is similar to that

obtained from previous studies [20-23]. In the polycrystalline phases, it is clear that the heat flux

parallel to the layers is greater than that across the $InO_2^-/GaO(ZnO)_m^+$ interfaces. This reduces

the $R$ values measured from the polycrystalline superlattices compared to the single crystalline values. Therefore, the $R_K$ calculated from polycrystalline superlattices is significantly underestimated than that calculated from single-crystalline superlattices.

These results also show that the $InO_2^-$ interfaces do not always increase the thermal resistance. The crossover between lines A and B in **Fig. 5b** as well as the sudden change in $R_K$ represent a change in the nature of scattering mechanism dominating the heat conduction from incoherent to coherent phonon scattering, which was also reported in artificial superlattices[24]. Most of the phonons in $GaO(ZnO)_m^+$ blocks are diffusely scattered at the $InO_2^-/GaO(ZnO)_m^+$ interface due to the discontinuity in the phonon density of states (DOS) from the mismatch between the force constants associated with the atomic bonds, which significantly suppresses the heat conduction. Once $d_{SL}$ reaches a certain threshold, diffuse scattering processes no longer affect the overall heat conduction as they are all blocked at the $InO_2^-$ interfaces. In this case, the heat conduction is dominated by long-wavelength phonons that maintain their momentum as well as phase through propagation[45]. These phonons are not diffusely scattered at interfaces and mainly affected by the wave-like nature of phonons. With increasing number of atomic planes between adjacent $InO_2^-/GaO(ZnO)_m^+$ interfaces, the phonon band folding decreases the phonon group velocity due to the opening of phonon band gaps at the edges of mini-Brillouin zones[24, 46]. Therefore, as the interface density increases, the Brillouin zone will expand, and the abovementioned gaps at the zone edge will close, which increases the group velocity and the thermal conductivity. The interface scattering (line A) represents the particle-like (diffusive) nature of phonons while the group velocity reflects the wave-like nature (specular) of phonons (line B).

According to **Fig. 5**, the crossover between the particle-like (diffuse) and wave-like (specular) phonon behaviors occurs at $d_{SL} = 2.0$ nm, which likely corresponds to the phonon coherence

length of $InGaO_3(ZnO)_m$. Regardless of the directions ($\kappa_\perp$, $\kappa_\parallel$), when the $d_{SL}$ is shorter than the phonon coherence length, the phonon propagation is dominated by the wave-like nature and the heat conduction becomes coherent. In other words, the phonon transport properties become coherent below $m = 5$[24, 46]. On the other hand, if $d_{SL}$ is longer than the coherence length, the wave-like characteristics of phonons are suppressed, and the phonon scattering becomes diffusive, which is incoherent. This phenomenon was predicted and observed from alternatively stacked layers consist of multi-atomic planes[24], but our results demonstrate that the same heat conduction mechanism is valid for superstructures with atomically thin layers as well. This provides an interesting insight on utilizing the properties of these structures. For designing a better thermal conductor, it is trivial that the interfaces need to be avoided. However, interface density densities need to be adequately controlled for achieving the minimum thermal conductivity.

In summary, we observed an ultralow thermal conductivity $\kappa$ (~1 W m$^{-1}$ K$^{-1}$) in single crystalline $InGaO_3(ZnO)_m$ superlattices, which is lower than random-oriented polycrystalline materials. This unexpected behavior is attributed to the presence of large Kapitza resistance $R_K$ at interfaces arranged in an atomic scale. Furthermore, the thermal resistance is strongly dependent on the layer thickness due to the phonon coherent length of $InGaO_3(ZnO)_m$. A minimum $\kappa$ of 1.1 W m$^{-1}$ K$^{-1}$ ($m = 4, 5$) is obtained, which is approximately 1/3 of the polycrystalline ceramic $InGaO_3(ZnO)_m$. Along the parallel direction, $\kappa_\parallel$ exhibited a decreasing tendency with decreasing $m$ values, then plateaued when $d_{SL}$ matched the phonon coherence length, indicating a change in the main scattering mechanism from diffuse to specular scattering. In both directions, the change in the scattering mechanism occurred when $d_{SL}$ became comparable to the phonon coherent length. The present results showed that the intrinsic Kapitza resistance in superlattices can be more effective in reducing $\kappa$ then grain boundaries in certain material systems. The fundamental heat transport characteristics of

InGaO$_3$(ZnO)$_m$ could be essential for implementing this class in materials for advanced thermal management technologies.

**Experimental Section**

*Single-crystalline film growth of InGaO$_3$(ZnO)$_m$*: The InGaO$_3$(ZnO)$_m$ ($m$ = 1−35) single crystalline films were fabricated by the reactive solid-phase epitaxy (R-SPE) method[25, 32, 33] on (111)- or (110) oriented yttria-stabilized zirconia (YSZ) single crystalline substrate. Firstly, ZnO film was heteroepitaxially grown on (111)- or (110)- surface of YSZ at 600 °C. Then, the film was cooled to room temperature, and amorphous InGaO$_3$(ZnO)$_m$ were deposited on the ZnO film. The bilayer film was heated up to 1400 °C in air for 30 min while the film was fully covered by another YSZ plate to suppress the vaporization of ZnO. The $m$-value was adjusted by controlling the ZnO thickness and the $m$-value of amorphous InGaO$_3$(ZnO)$_m$ thickness ratio. Detailed descriptions about our R-SPE method were published elsewhere[25, 32, 33].

*Structural analyses of the films*: High resolution X-ray diffraction (HRXRD, Cu Kα$_1$ radiation, ATX-G, Rigaku Co.) was used to measure the thickness, the superlattice period ($d_{SL}$), $m$-value, and the average tilt angle of the resultant InGaO$_3$(ZnO)$_m$ films. An atomic force microscopy (AFM, Nanocute, Hitachi-Hightechnol. Co.) was used to observe the surface morphology of the films. High-angle annular dark field (HAADF) scanning transmission electron microscopy (STEM) was used to observe the atomic arrangement of the films.

*Thermal conductivity measurement of the films*: The thermal conductivity $\kappa$ was calculated from $\kappa = \alpha \cdot C_p \cdot \rho$, where $\alpha$ is the thermal diffusivity, $C_p$ is the specific heat capacity, and $\rho$ is the density of the sample, respectively. The out-of-plane $\alpha$ of the R-SPE grown single

crystalline $InGaO_3(ZnO)_m$ films were measured by the time-domain thermoreflectance (TDTR, Front heating/Front detection mode−Mirror image method, PicoTR, PicoTherm Co.[47]) method at room temperature (**Fig. 2**, **Supplementary Fig. S1**). Sputtered Mo films (thickness: ~100 nm) were used as a transducer. The samples were irradiated with femtosecond laser pulses (wavelength: 1550 nm, pulse duration: 0.5 ps), and the change in the reflectivity in the time domain was recorded with a probe laser (wavelength: 775 nm, pulse duration: 0.5 ps). The obtained thermoreflectance signals were analyzed with a software package provided by the manufacturer (PicoThem Co.[47]). For more details of our TDTR measurement, see **Supplementary Fig. S1** and the explanation.

**Supporting Information**
Supporting Information is available from the Wiley Online Library or from the author.

Received: ((will be filled in by the editorial staff))
Revised: ((will be filled in by the editorial staff))
Published online: ((will be filled in by the editorial staff))

**References**

[1]     G. J. Snyder, E. S. Toberer, *Nat. Mater.* **2008**, *7*, 105-114.

[2]     J. He, T. M. Tritt, *Science* **2017**, *357*, eaak9997.

[3]     N. P. Padture, M. Gell, E. H. Jordan, *Science* **2002**, *296*, 280-284.

[4]     D. R. Clarke, S. R. Phillpot, *Mater. Today* **2005**, *8*, 22-29.

[5]     R. Vassen, M. O. Jarligo, T. Steinke, D. E. Mack, D. Stover, *Surf. Coat. Technol.* **2010**, *205*, 938-942.

[6]     N. P. Padture, *Nat. Mater.* **2016**, *15*, 804-809.

[7]     G. L. Pollack, *Rev. Mod. Phys.* **1969**, *41*, 48-81.

[8]     D. G. Cahill, P. V. Braun, G. Chen, D. R. Clarke, S. H. Fan, K. E. Goodson, P. Keblinski, W. P. King, G. D. Mahan, A. Majumdar, H. J. Maris, S. R. Phillpot, E. Pop, L. Shi, *Appl. Phys. Rev.* **2014**, *1*, 011305.

[9]     T. D. Sparks, P. A. Fuierer, D. R. Clarke, *J. Am. Ceram. Soc.* **2010**, *93*, 1136-1141.

[10]    Y. Shen, D. R. Clarke, P. A. Fuierer, *Appl. Phys. Lett.* **2008**, *93*, 102907.

[11]    D. G. Cahill, M. Katlyar, J. R. Abelson, *Phys. Rev. B* **1994**, *50*, 6077.

[12]    D. G. Cahill, S. K. Watson, R. O. Pohl, *Phys. Rev. B* **1992**, *46*, 6131.

[13]    J. Feng, B. Xiao, R. Zhou, W. Pan, D. R. Clarke, *Acta Mater.* **2012**, *60*, 3380-3392.

[14]    E. Hadland, H. Jang, M. Falmbigl, R. Fischer, D. L. Medlin, D. G. Cahill, D. C. Johnson, *Chem. Mater.* **2019**, *31*, 5699-5705.

[15]    E. Hadland, H. Jang, N. Wolff, R. Fischer, A. C. Lygo, G. Mitchson, D. Li, L. Kienle, D. G. Cahill, D. C. Johnson, *Nanotechnology* **2019**, *30*, 285401.

[16]    C. Chiritescu, D. G. Cahill, N. Nguyen, D. Johnson, A. Bodapati, P. Keblinski, P. Zschack, *Science* **2007**, *315*, 351-353.

[17]    N. S. Gunning, J. Feser, M. Falmbigi, M. Beekman, D. G. Cahill, D. C. Johnson, *Semicond. Sci. Technol.* **2014**, *29*, 124007.

[18]    N. S. Gunning, J. Feser, M. Beekman, D. G. Cahill, D. C. Johnson, *J. Am. Ceram. Soc.* **2015**, *137*, 8803-8809.

[19]    A. Chernatynskiy, R. W. Grimes, M. A. Zurbuchen, D. R. Clarke, S. R. Phillpot, *Appl. Phys. Lett.* **2009**, *95*, 161906.

[20]    H. Kasper, *Z. Anorg. Allg. Chem.* **1967**, *349*, 113-123.

[21]   P. J. Cannard, R. J. D. Tilley, *J. Solid State Chem.* **1988**, *73*, 418-426.

[22]   M. Nakamura, N. Kimizuka, T. Mohri, *J. Solid State Chem.* **1990**, *86*, 16-40.

[23]   C. F. Li, Y. Bando, M. Nakamura, M. Onoda, N. Kimizuka, *J. Solid State Chem.* **1998**, *139*, 347-355.

[24]   J. Ravichandran, A. K. Yadav, R. Cheaito, P. B. Rossen, A. Soukiassian, S. J. Suresha, J. C. Duda, B. M. Foley, C. H. Lee, Y. Zhu, A. W. Lichtenberger, J. E. Moore, D. A. Muller, D. G. Schlom, P. E. Hopkins, A. Majumdar, R. Ramesh, M. A. Zurbuchen, *Nat. Mater.* **2014**, *13*, 168-172.

[25]   H. Ohta, K. Nomura, M. Orita, M. Hirano, K. Ueda, T. Suzuki, Y. Ikuhara, H. Hosono, *Adv. Funct. Mater.* **2003**, *13*, 139-144.

[26]   S. W. Cho, S. K. Baek, D. E. Kim, Y. Kim, H. K. Cho, *J. Vac. Sci. Technol. A* **2017**, *35*, 01B126.

[27]   B. Cui, D. B. Buchholz, L. Zeng, M. Bedzyk, *MRS Adv.* **2016**, *1*, 1631-1636.

[28]   B. Cui, L. Zeng, D. Keane, M. J. Bedzyk, D. B. Buchholz, R. P. H. Chang, X. Yu, J. Smith, T. J. Marks, Y. Xia, A. F. Facchetti, J. E. Medvedeva, M. Grayson, *J. Phys. Chem. C* **2016**, *120*, 7467-7475.

[29]   X. Liang, M. Baram, D. R. Clarke, *Appl. Phys. Lett.* **2013**, *102*, 223903.

[30]   H. J. Cho, G. Kim, T. Onozato, H. Jeen, H. Ohta, *Int. J. Heat Mass Transf.* **2019**, *137*, 263-267.

[31]   H. J. Cho, Y. Takashima, Y. Nezu, T. Onozato, H. Ohta, *Adv. Mater. Interfaces* **2020**, *7*, 1901816.

[32]   K. Nomura, H. Ohta, K. Ueda, T. Kamiya, M. Hirano, H. Hosono, *Science* **2003**, *300*, 1269-1272.

[33]   K. Nomura, H. Ohta, K. Ueda, T. Kamiya, M. Orita, M. Hirano, T. Suzuki, C. Honjyo, Y. Ikuhara, H. Hosono, *J. Appl. Phys.* **2004**, *95*, 5532-5539.

[34]   H. Ohta, W. S. Seo, K. Koumoto, *J. Am. Ceram. Soc.* **1996**, *79*, 2193-2196.

[35]    L. D. Zhao, Y. L. Pei, Y. Liu, D. Berardan, N. Dragoe, *J. Am. Ceram. Soc.* **2011**, *94*, 1664-1666.

[36]    X. Liang, M. Baram, D. R. Clarke, *Appl. Phys. Lett.* **2013**, *102*, 223903.

[37]    X. X. Zhang, H. J. Wu, Y. L. Pei, Y. M. Zhou, S. K. Gong, J. Q. He, L. D. Zhao, *Acta Mater.* **2017**, *136*, 235-241.

[38]    W. D. Thompson, B. E. White, *J. Electron. Mater.* **2016**, *45*, 4890-4897.

[39]    F. Krahl, Y. Z. Wu, H. J. Cho, M. Karppinen, H. Ohta, *Adv. Electron. Mater.* **2020**, *6,* 2000404.

[40]    G. Chen, *J. Heat Transf.* **1997**, *119*, 220-229.

[41]    K. Termentzidis, P. Chantrenne, *Phys. Rev. B* **2009**, *79*, 214307.

[42]    G. Chen, M. Neagu, *Appl. Phys. Lett.* **1997**, *71*, 2761-2763.

[43]    S. M. Lee, D. G. Cahill, R. Venkatasubramanian, *Appl. Phys. Lett.* **1997**, *70*, 2957-2959.

[44]    Y. K. Koh, Y. Cao, D. G. Cahill, D. Jena, *Adv. Funct. Mater.* **2009**, *19*, 610-615.

[45]    M. N. Luckyanova, J. Garg, K. Esfarjani, A. Jandl, M. T. Bulsara, A. J. Schmidt, A. J. Minnich, S. Chen, M. S. Dresselhaus, Z. F. Ren, E. A. Fitzgerald, G. Chen, *Science* **2012**, *338*, 936-939.

[46]    M. V. Simkin, G. D. Mahan, *Phys. Rev. Lett.* **2000**, *84*, 927-930.

[47]    S. H. Firoz, T. Yagi, N. Taketoshi, K. Ishikawa, T. Baba, *Meas. Sci. Technol.* **2011**, *22*, 024012.

[48]    S. Preaud, C. Byl, F. Brisset, D. Berardan, *J. Am. Ceram. Soc.* **2020**, *103*, 3030-3038.
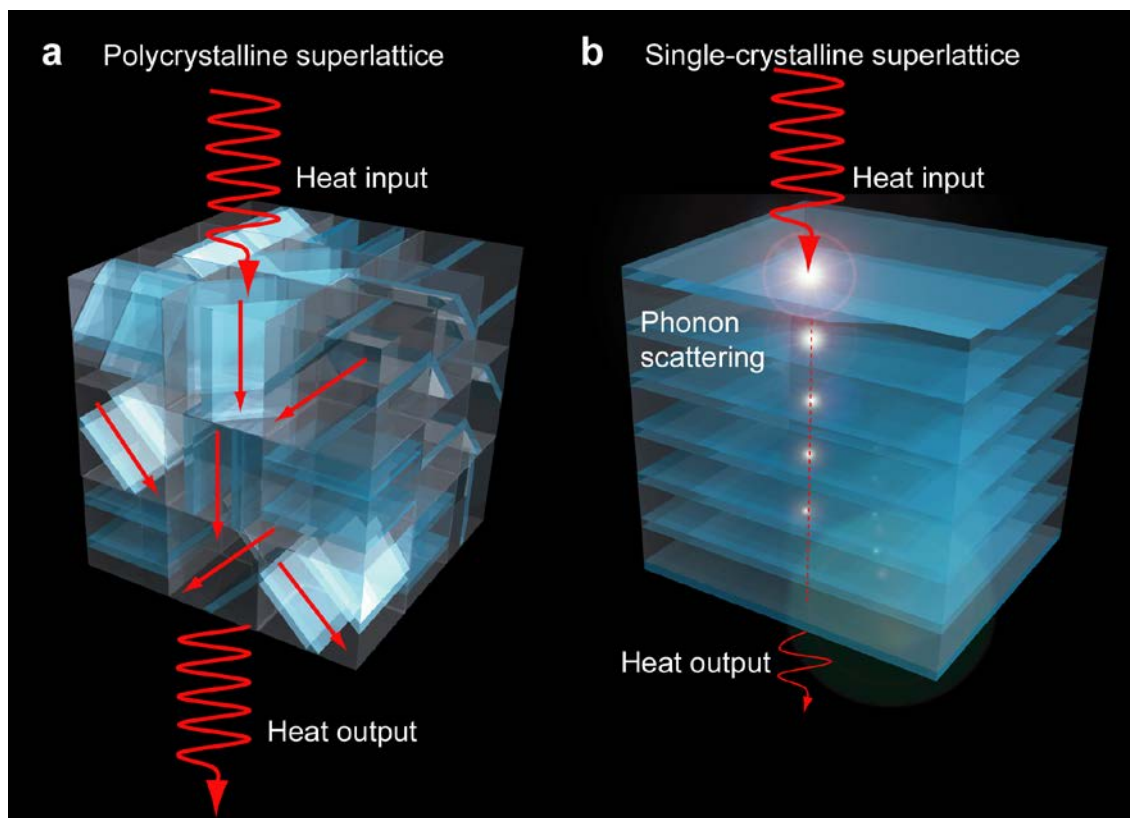
**Figure 1.** Difference in the heat conduction for the thermodynamically formed (a) polycrystalline and (b) single-crystalline superlattices. In the case of randomly oriented polycrystalline superlattices (a), thermal transport predominantly occurs parallel to the layers where continuous phonon propagation is allowed in the long wavelength limit. This does not strongly suppress the conduction of heat. On the other hand, in the case of single crystalline superlattices (b), heat conduction requires multiple phonon conversions (particle-like) or partial transmissions and partial reflections (wave-like) at many interfaces, leading to discontinuous phonon propagation. Therefore, all phonons experience significant scatterings from the interfaces, i.e., diffusive scattering from the former and specular scattering from the latter, and the conduction of heat is strongly suppressed (Kapitza resistance).
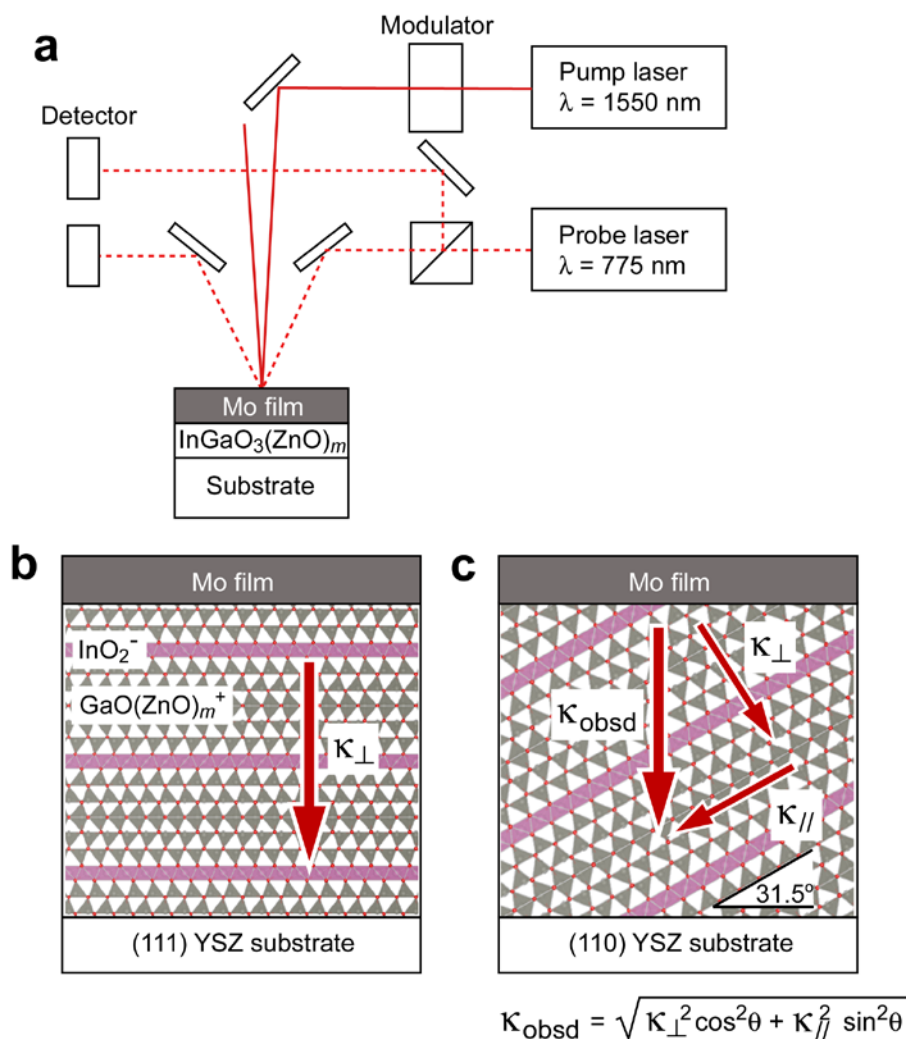
**Figure 2.** Approach to measure the anisotropy of thermal conductivity for superlattices. (a) Schematic optical arrangement of the time-domain thermoreflectance measurement. The decay of reflectance signal of probe laser was measured using a Mo film as the transducer deposited on the surface of $InGaO_3(ZnO)_m$ films. (b)(c) Schematic crystal structure of $InGaO_3(ZnO)_4$ grown on (b) (111) YSZ substrate and (c) (110) YSZ substrate. We extracted thermal conductivity along the layer ($\kappa_{//}$) using the thermal conductivity values of $\kappa\perp$ from (b) and $\kappa_{obsd}$ from (c). The $\theta$ value is 31.5°.
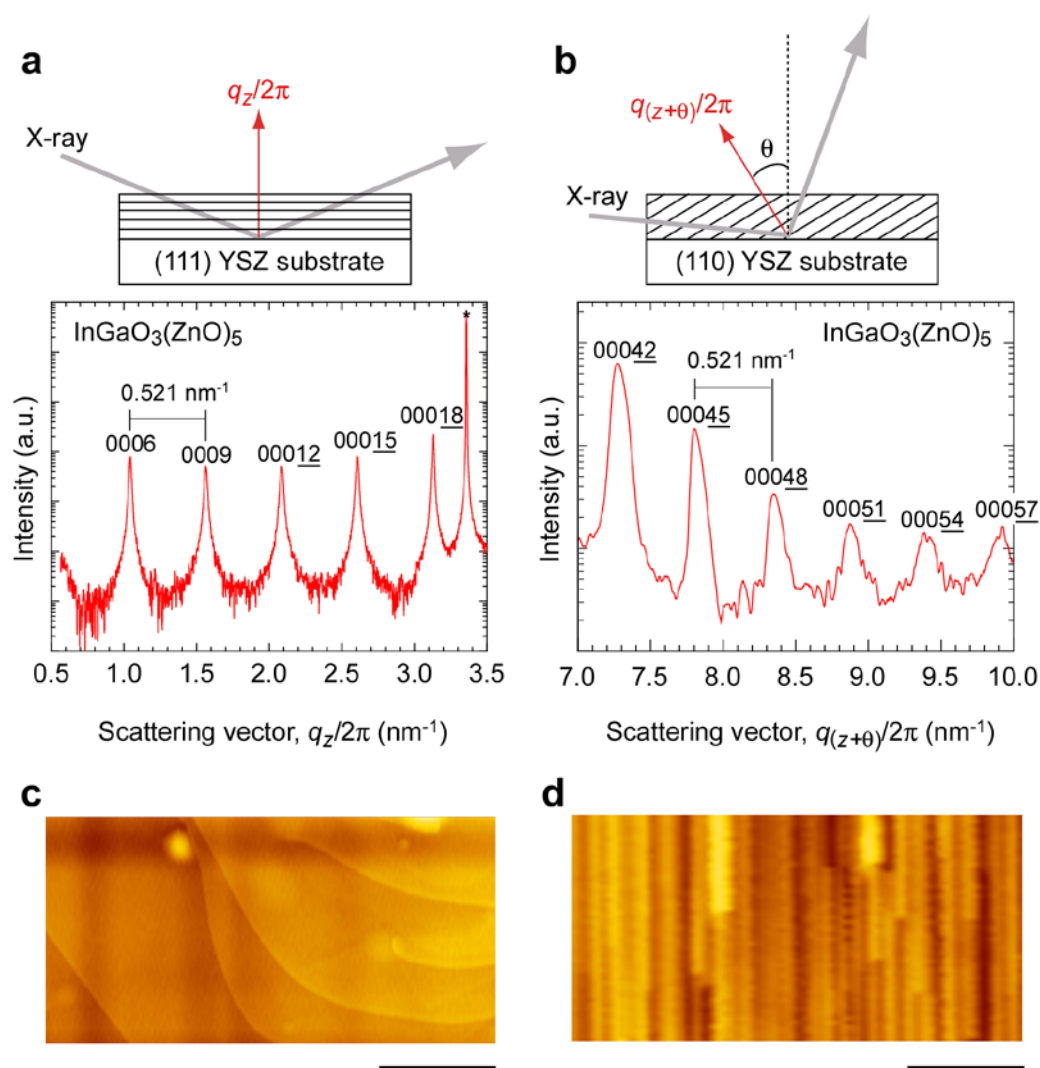
**Figure 3.** X-ray diffraction analyses of the superlattices. (a) Out-of-plane XRD pattern of the resultant InGaO$_3$(ZnO)$_5$ film on (111) YSZ substrate. Intense diffraction peaks of 000$l$ InGaO$_3$(ZnO)$_m$ are seen together with 111 YSZ substrate (*). (b) Off-axis XRD pattern of the resultant InGaO$_3$(ZnO)$_5$ film on (110) YSZ substrate. Intense diffraction peaks of 000$l$ InGaO$_3$(ZnO)$_m$ are seen when $\theta = 31.5°$. The peak interval (0.521 nm$^{-1}$) corresponds to the distance between two adjacent InO$_2^-$ layers (1.92 nm). (c)(d) Topographic AFM images of InGaO$_3$(ZnO)$_5$ film on (c) (111) YSZ substrate and (d) (110) YSZ substrate. The scale bar is 500 nm.
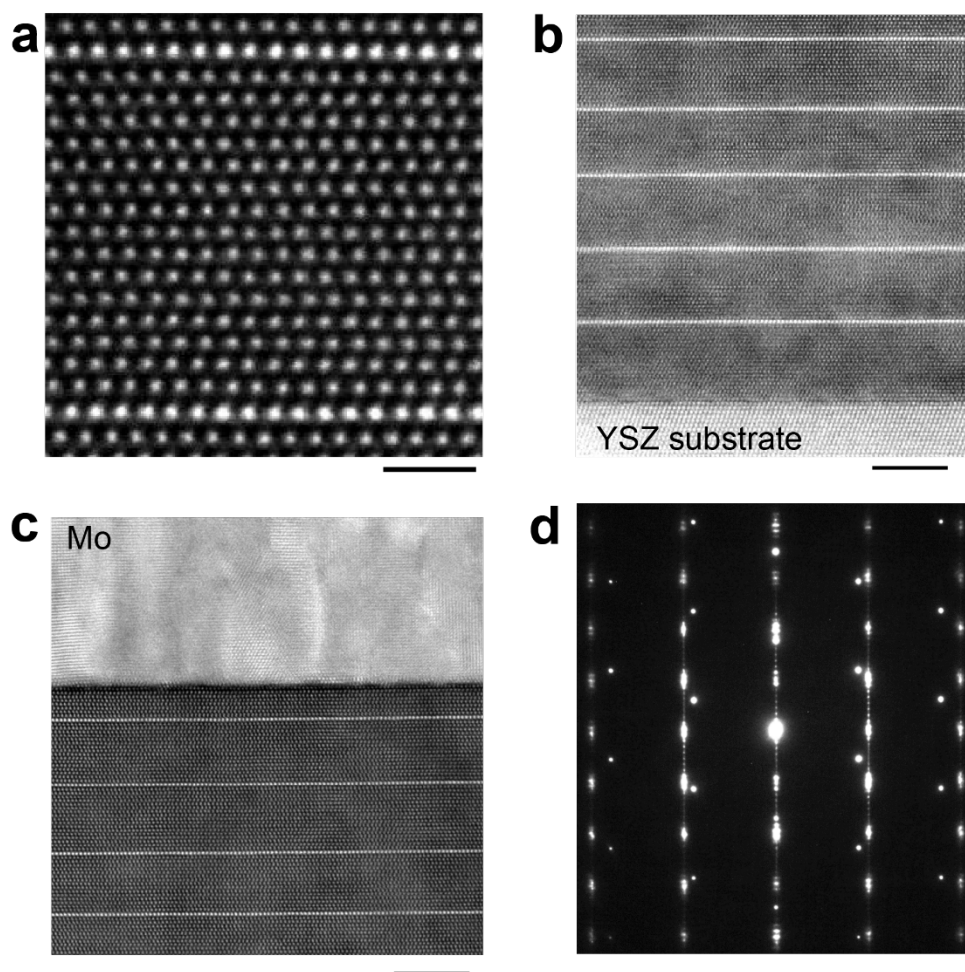
**Figure 4.** Atomic arrangement of the superlattices. (a−c) Cross-sectional HAADF-STEM images of the resultant $InGaO_3(ZnO)_m$ film ($m = 15$) grown on (111) YSZ single crystal substrate. Brighter lines of one-atomic-layer thickness periodically present, corresponding to $InO_2^-$ layers. (a) atomic structure of the layered structure (scale bar = 1 nm). (b) the bottom part (scale bar = 5 nm) and (c) the top part of the film (scale bar = 5 nm). (d) Selected area electron diffraction pattern of the $InGaO_3(ZnO)_m$ film.
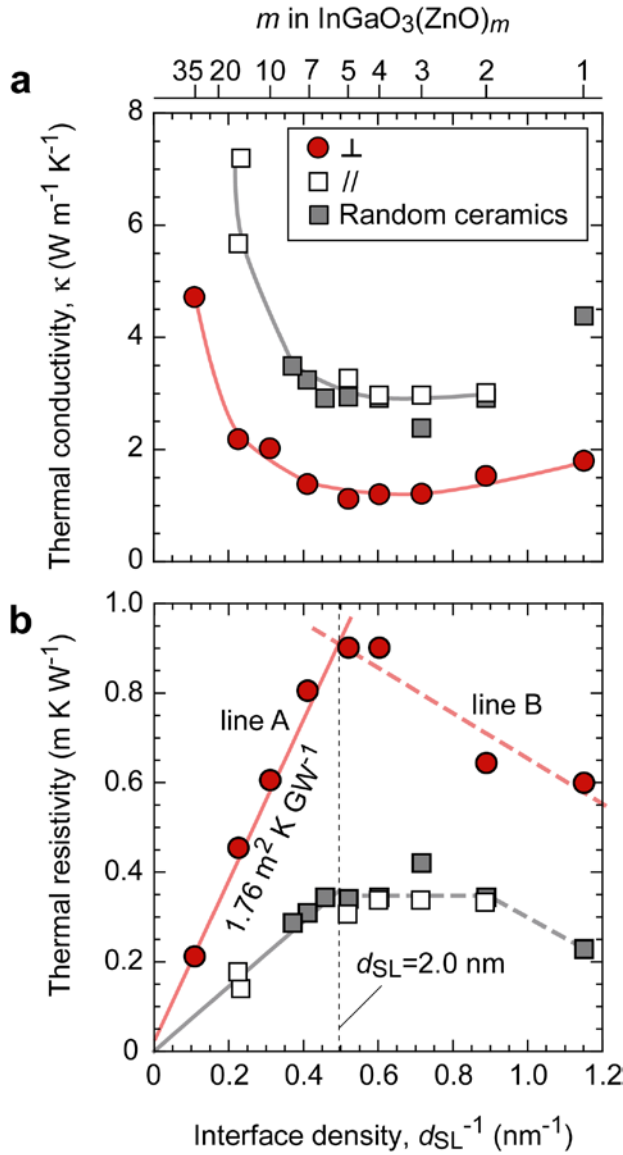
**Figure 5.** Anomalously low thermal conductivity perpendicular (⊥) to the superlattices. (a) Thermal conductivity ($\kappa$) of the resultant $InGaO_3(ZnO)_m$ films ($\kappa\perp$: perpendicular to the superlattice, $\kappa_{//}$: parallel to the superlattice) as a function of the interface density, $d_{SL}^{-1}$. The $\kappa$-values for randomly-oriented polycrystalline ceramics of $InGaO_3(ZnO)_m$ (gray squares: $m = 1-9$[48]) are also plotted for comparison. The thermal conductivity values of random ceramics are similar to those of $\kappa_{//}$, indicating that the phonon propagation parallel to the superlattice dominates the heat conduction of random ceramics. The errors, which came from the noise of the TDTR signal, ranged from 5 – 15 % but omitted since they were often smaller than the size of the symbol. (b) Thermal resistivity plots as a function of the interface density, $d_{SL}^{-1}$. Two straight lines A and B could be drawn to indicate the crossover of incoherent to coherent phonon propagation (see text for the detail). The $d_{SL}$ at the crossover point between the line is 2.0 nm. The Kapitza resistance and the thermal conductivity of $GaO(ZnO)_m^+$ block ($m = \infty$) were extracted to be 1.76 $m^2$ K $GW^{-1}$ and 20.9 W $m^{-1}$ $K^{-1}$, respectively.

Anomalously low heat conduction in perpendicular to the single-crystal natural superlattice $InGaO_3(ZnO)_m$ was found. The thermal conductivity ($\kappa$) was only 1.1 W m$^{-1}$ K$^{-1}$, ~1/3 of randomly-oriented polycrystals of $InGaO_3(ZnO)_m$. The large difference in $\kappa$ was due to the large $\kappa$ parallel to the natural superlattice. The present results would be useful for the material design of thermal management technologies.

**Keyword** thermal management technologies, thermal conductivity, superlattice, $InGaO_3(ZnO)_m$, Kapitza resistance

H.J. Cho*, Y. Wu, Y. Zhang, B. Feng, M. Mikami, W. Shin, Y. Ikuhara, Y.-M. Sheu, K. Saito, and H. Ohta*

**Anomalously Low Heat Conduction in Single-Crystal Superlattice Ceramics Lower than Randomly Oriented Polycrystals**

WILEY-VCH
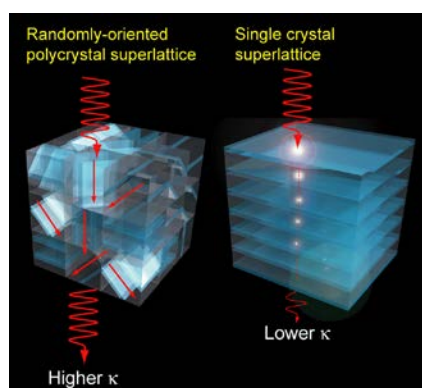
Supporting Information

**Anomalously Low Heat Conduction in Single-Crystal Superlattice Ceramics Lower than Randomly Oriented Polycrystals**

*Hai Jun Cho\*, Yuzhang Wu, Yu-qiao Zhang, Bin Feng, Masashi Mikami, Woosuck Shin, Yuichi Ikuhara, Yu-Miin Sheu, Keiji Saito, and Hiromichi Ohta\**

**Table S1.** Summary of the thermal conductivity measurement of the InGaO$_3$(ZnO)$_m$ films grown on (111)-oriented YSZ substrates. $m$-values, film thickness ($t$), the superlattice periods ($d_{SL}$)(obsd.: observed, calcd.: calculated), the density ($\rho$), the specific heat capacity ($C_p$), thermal diffusivity ($\alpha$), thermal conductivity ($\kappa$), Kapitza resistance at the Mo/InGaO$_3$(ZnO)$_m$ interface ($R_{K\text{-Mo/Film}}$), and InGaO$_3$(ZnO)$_m$/YSZ interface ($R_{K\text{-Film/Substrate}}$) are listed.

| $m$-value | 1 | 2 | 4 | 5 | 7 |
|---|---|---|---|---|---|
| $t$ (nm) | 91 | 278 | 143 | 177 | 217 |
| $d_{SL\text{ obsd.}}$ (nm) | 0.8749 | 1.137 | 1.659 | 1.921 | 2.438 |
| $d_{SL\text{ calcd.}}$ (nm) | 0.8658 | 1.126 | 1.6452 | 1.9050 | 2.4246 |
| $\rho$ (g·cm$^{-3}$) | 6.404 | 6.239 | 6.036 | 5.987 | 5.922 |
| $C_p$ (J·kg$^{-1}$·K$^{-1}$) | 441 | 459 | 479 | 486 | 494 |
| $\alpha$ (m$^2$·s$^{-1}$) | $5.88 \times 10^{-7}$ | $5.20 \times 10^{-7}$ | $3.80 \times 10^{-7}$ | $3.81 \times 10^{-7}$ | $4.17 \times 10^{-7}$ |
| $\kappa$ (W·m$^{-1}$·K$^{-1}$) | 1.65 | 1.50 | 1.10 | 1.10 | 1.20 |
| $R_{K\text{-Mo/Film}}$ (m$^2$·K·GW$^{-1}$) | $2.20 \times 10^{-9}$ | $1.0 \times 10^{-9}$ | $1.0 \times 10^{-9}$ | $4.0 \times 10^{-9}$ | $1.0 \times 10^{-9}$ |
| $R_{K\text{-Film/Substrate}}$ (m$^2$·K·GW$^{-1}$) | $1.0 \times 10^{-9}$ | $1.0 \times 10^{-9}$ | $1.0 \times 10^{-9}$ | $1.0 \times 10^{-9}$ | $1.0 \times 10^{-9}$ |

| $m$-value | 10 | 15 | 35 |
|---|---|---|---|
| $t$ (nm) | 223 | 261 | 200 |
| $d_{SL\text{ obsd.}}$ (nm) | 3.219 | 4.358 | 10.01 |
| $d_{SL\text{ calcd.}}$ (nm) | 3.204 | 4.503 | 9.699 |
| $\rho$ (g·cm$^{-3}$) | 5.867 | 5.817 | 5.753 |
| $C_p$ (J kg$^{-1}$·K$^{-1}$) | 502 | 510 | 520 |
| $\alpha$ (m$^2$·s$^{-1}$) | $5.64 \times 10^{-7}$ | $6.74 \times 10^{-7}$ | $1.6 \times 10^{-6}$ |
| $\kappa$ (W·m$^{-1}$·K$^{-1}$) | 1.65 | 2.00 | 4.80 |
| $R_{K\text{-Mo/Film}}$ (m$^2$·K·GW$^{-1}$) | $1.0 \times 10^{-9}$ | $1.0 \times 10^{-9}$ | $3.0 \times 10^{-9}$ |
| $R_{K\text{-Film/Substrate}}$ (m$^2$·K·GW$^{-1}$) | $1.0 \times 10^{-9}$ | $1.0 \times 10^{-9}$ | $1.0 \times 10^{-9}$ |

**Table S2.** Summary of the thermal conductivity measurement of the InGaO$_3$(ZnO)$_m$ films grown on (110)-oriented YSZ. $m$-values, film thickness ($t$), the superlattice periods ($d_{SL}$)(obsd.: observed, calcd.: calculated), the density ($\rho$), the specific heat capacity ($C_p$), thermal diffusivity ($\alpha$), thermal conductivity ($\kappa$), Kapitza resistance at the Mo/InGaO$_3$(ZnO)$_m$ interface ($R_{K\text{-Mo/Film}}$), and InGaO$_3$(ZnO)$_m$/YSZ interface ($R_{K\text{-Film/Substrate}}$) are listed.

| $m$-value | 2 | 3 | 4 | 5 | 14 |
|---|---|---|---|---|---|
| $t$ (nm) | 169 | 94 | 112 | 102 | 66 |
| $d_{SL\ obsd.}$ (nm) | 1.1284 | 1.3981 | 1.6689 | 1.8966 | 4.4303 |
| $d_{SL\ calcd.}$ (nm) | 1.1256 | 1.3854 | 1.6452 | 1.905 | 4.2432 |
| $\rho$ (g·cm$^{-3}$) | 6.239 | 6.105 | 6.036 | 5.987 | 5.825 |
| $C_p$ (J·kg$^{-1}$·K$^{-1}$) | 459 | 471 | 479 | 486 | 508 |
| $\alpha$ (m$^2$·s$^{-1}$) | $6.98 \times 10^{-7}$ | $6.26 \times 10^{-7}$ | $6.27 \times 10^{-7}$ | $6.53 \times 10^{-7}$ | $1.52 \times 10^{-6}$ |
| $\kappa$ (W·m$^{-1}$·K$^{-1}$) | 2.0 | 1.8 | 1.8 | 1.9 | 4.5 |
| $\kappa_{//}$ (W·m$^{-1}$·K$^{-1}$) | 3.01 | 2.97 | 2.97 | 3.27 | 7.19 |
| $R_{K\text{-Mo/Film}}$ (m$^2$·K·GW$^{-1}$) | $5.0 \times 10^{-9}$ | $4.0 \times 10^{-9}$ | $7.0 \times 10^{-9}$ | $8.0 \times 10^{-9}$ | $1.5 \times 10^{-8}$ |
| $R_{K\text{-Film/Substrate}}$ (m$^2$·K·GW$^{-1}$) | $1.0 \times 10^{-9}$ | $1.0 \times 10^{-9}$ | $1.0 \times 10^{-9}$ | $2.0 \times 10^{-9}$ | $1.0 \times 10^{-9}$ |

| $m$-value | 15 |
|---|---|
| $t$ (nm) | 70 |
| $d_{SL\ obsd.}$ (nm) | 4.7621 |
| $d_{SL\ calcd.}$ (nm) | 4.503 |
| $\rho$ (g·cm$^{-3}$) | 5.817 |
| $C_p$ (J kg$^{-1}$·K$^{-1}$) | 510 |
| $\alpha$ (m$^2$·s$^{-1}$) | $1.28 \times 10^{-6}$ |
| $\kappa$ (W·m$^{-1}$·K$^{-1}$) | 3.8 |
| $\kappa_{//}$ (W·m$^{-1}$·K$^{-1}$) | 5.67 |
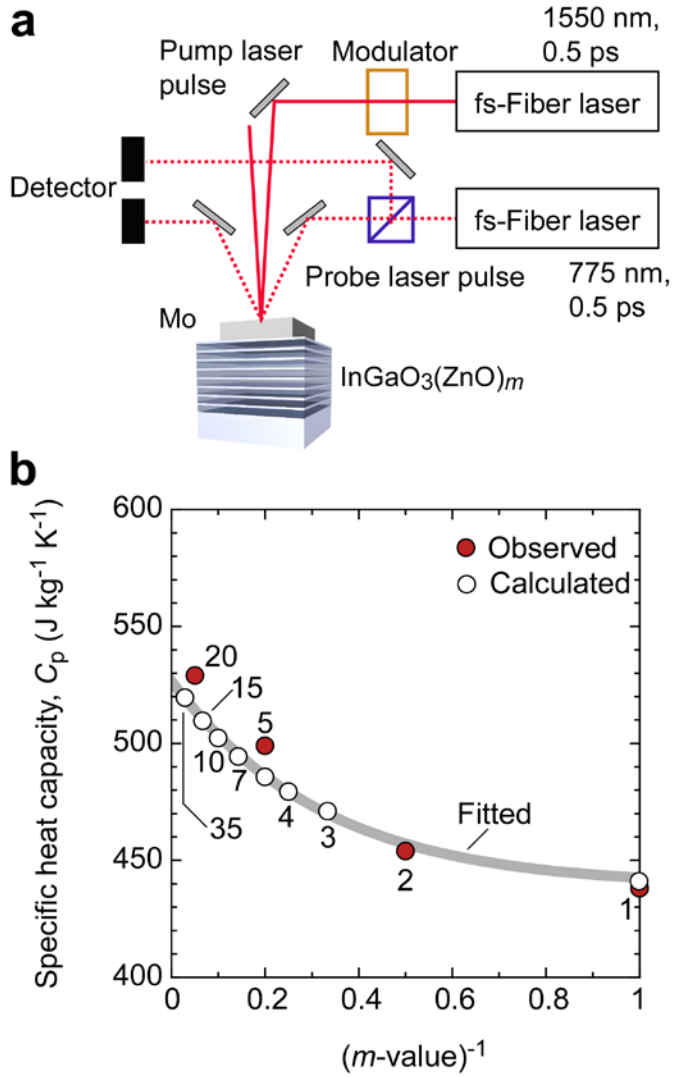
**Figure S1.** Thermal conductivity measurement from the TDTR method. (a) The thermal diffusivity (α) of the single crystalline InGaO$_3$(ZnO)$_m$ films in the cross-plane direction (perpendicular to the superlattice) was measured by the time-domain thermoreflectance (TDTR, PicoTR, PicoTherm Co.[46]) method at room temperature. Sputtered Mo films (thickness: ~100 nm) were used as the transducer. The samples were irradiated with femtosecond laser pulses (wavelength: 1550 nm, pulse duration: 0.5 ps), and the change in the reflectivity in the time domain was recorded with a probe laser (wavelength: 775 nm, pulse duration: 0.5 ps). (b) Specific heat of InGaO$_3$(ZnO)$_m$. Red circle: observed using the ceramic samples, white circle: calculated by using the following equation, the solid line: fitted by using the calculated values.

$$C_P = \sum_{i=1}^{N} C_{Pi} \cdot f_i = C_{P\,In_2O_3} \cdot f_{In_2O_3} + C_{P\,Ga_2O_3} \cdot f_{Ga_2O_3} + C_{P\,ZnO} \cdot f_{ZnO}$$

, where $f_i$ is the mass fraction of $i$-component. In order to simulate the observed data, we used the following $C_p$ values [In$_2$O$_3$: 357 J·kg$^{-1}$·K$^{-1}$,[48] Ga$_2$O$_3$: 490 J·kg$^{-1}$·K$^{-1}$,[49] ZnO: 528 J·kg$^{-1}$·K$^{-1}$ [50]] Since the calculated $C_p$ values well reproduce the observed values, we used the calculated $C_p$ values for the thermal conductivity calculation.

The temperature of the Mo transducer film at time ($t$) ($T_{FF}(t)$) is given the following equations:

25

$$T_{FF}(t) = \frac{1}{b_f \sqrt{\pi t}}\left(1 + 2\sum_{n=1}^{\infty}\gamma^n\left(-n^2\frac{\tau_f}{t}\right)\right)$$

$$\tau_f = \frac{d^2}{\alpha_f}$$

$$\gamma = \frac{b_m - b_f}{b_m + b_f}$$

, where $b_f$ is thermal effusivity ($= C_p \cdot \rho \cdot \alpha^{0.5}$), $\gamma$ is the multiplication coefficient for the amplitude of the virtual heat sources, $\tau_f$ is the heat diffusion time across the film, $d$ is the film thickness, respectively. The results are listed in Supplementary Table S1.

The $\alpha$ of the randomly-oriented polycrystalline $InGaO_3(ZnO)_m$ ($m$ = 1, 2, 5, and 20) ceramics were measured by the laser flash method at room temperature. The relative density of the ceramics were 94.6% for $m$ = 1, 90.6% for $m$ = 2, 92.9% for $m$ = 5, and 98.1% for $m$ = 20, respectively.

The $C_p$ of the $InGaO_3(ZnO)_m$ ($m$ = 1, 2, 5, and 20) was measured by the differential scanning calorimetry (DSC) at room temperature. The results are listed in the following table.

| $m$-value | 1 | 2 | 5 | 20 |
|---|---|---|---|---|
| $C_p$ (J·kg$^{-1}$·K$^{-1}$) | 438 | 454 | 499 | 529 |

We also calculated the $C_P$ using the following equation:

$$C_P = \sum_{i=1}^{N} C_{Pi} \cdot f_i = C_{P\,In_2O_3} \cdot f_{In_2O_3} + C_{P\,Ga_2O_3} \cdot f_{Ga_2O_3} + C_{P\,ZnO} \cdot f_{ZnO}$$

, where $f_i$ is the mass fraction of $i$-component. In order to simulate the observed data, we used following $C_p$ values [$In_2O_3$: 357 J·kg$^{-1}$·K$^{-1}$,[48] $Ga_2O_3$: 490 J·kg$^{-1}$·K$^{-1}$,[49] ZnO: 528 J·kg$^{-1}$·K$^{-1}$ [50]].
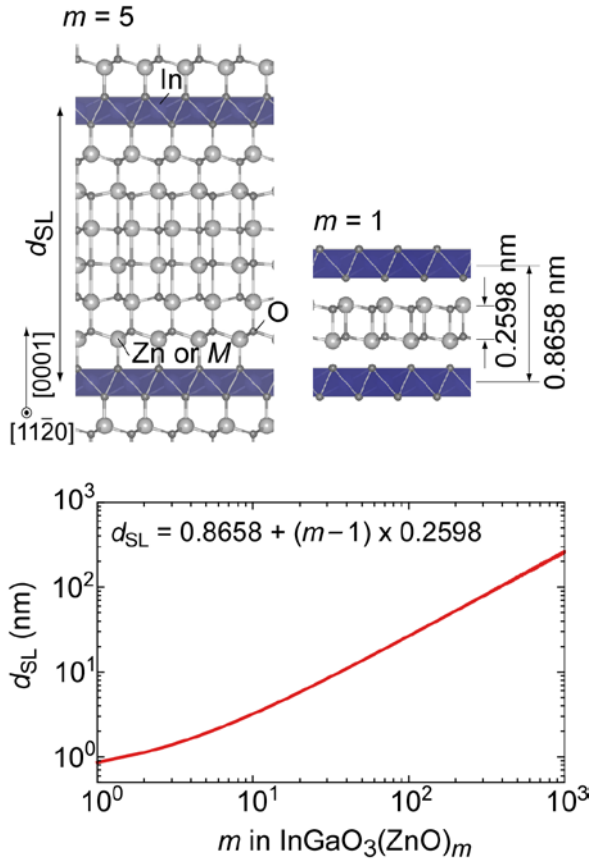
The $\rho$ of the InGaO$_3$(ZnO)$_m$ ($m$ = 1, 3, 4, 5, 7, 10, 15, and 35) were calculated from the following equation:

$$\rho = \frac{2MW}{N_A \cdot \sqrt{3} d_{SL} \cdot a^2}$$

, where $MW$ is the molecular weight of InGaO$_3$(ZnO)$_m$, $N_A$ is Avogadro constant, $d_{SL}$ is the superlattice period, and $a$ is the $a$-axis lattice parameter, respectively. The $d_{SL}$ of InGaO$_3$(ZnO)$_m$ is given by the following equation:[51]

$$d_{SL} = p + q + (m-1)r$$

where $p$ is the thickness of the InO$_2^-$ layer, $q$ is the thickness of the (Zn/Ga)O layer, and $r$ is the thickness of the ZnO layer. For InGaO$_3$(ZnO)$_m$, $p+q$ was 0.8658 nm, and $r$ was 0.2598 nm. The $a$-axis lattice parameter of InGaO$_3$(ZnO)$_m$ was obtained by the exponential fitting of the reported values[52] as a function of $m^{-1}$.

$$a = 0.32957 - 0.00481 e^{(m^{-1}/-0.18383)}$$

The obtained $a$-axis lattice parameters were 0.3295 nm for $m$ = 1, 0.3288 nm for $m$ = 3, 0.3283 nm for $m$ = 4, 0.3279 nm for $m$ = 5, 0.3274 nm for $m$ = 7, 0.3268 nm for $m$ = 10, 0.3262 nm for $m$ = 15, and 0.3255 nm for $m$ = 35, respectively. Using the $a$-axis lattice parameters and the $d_{SL}$, we theoretically calculated the density of InGaO$_3$(ZnO)$_m$ films. The results are listed in Supplementary Table S1.
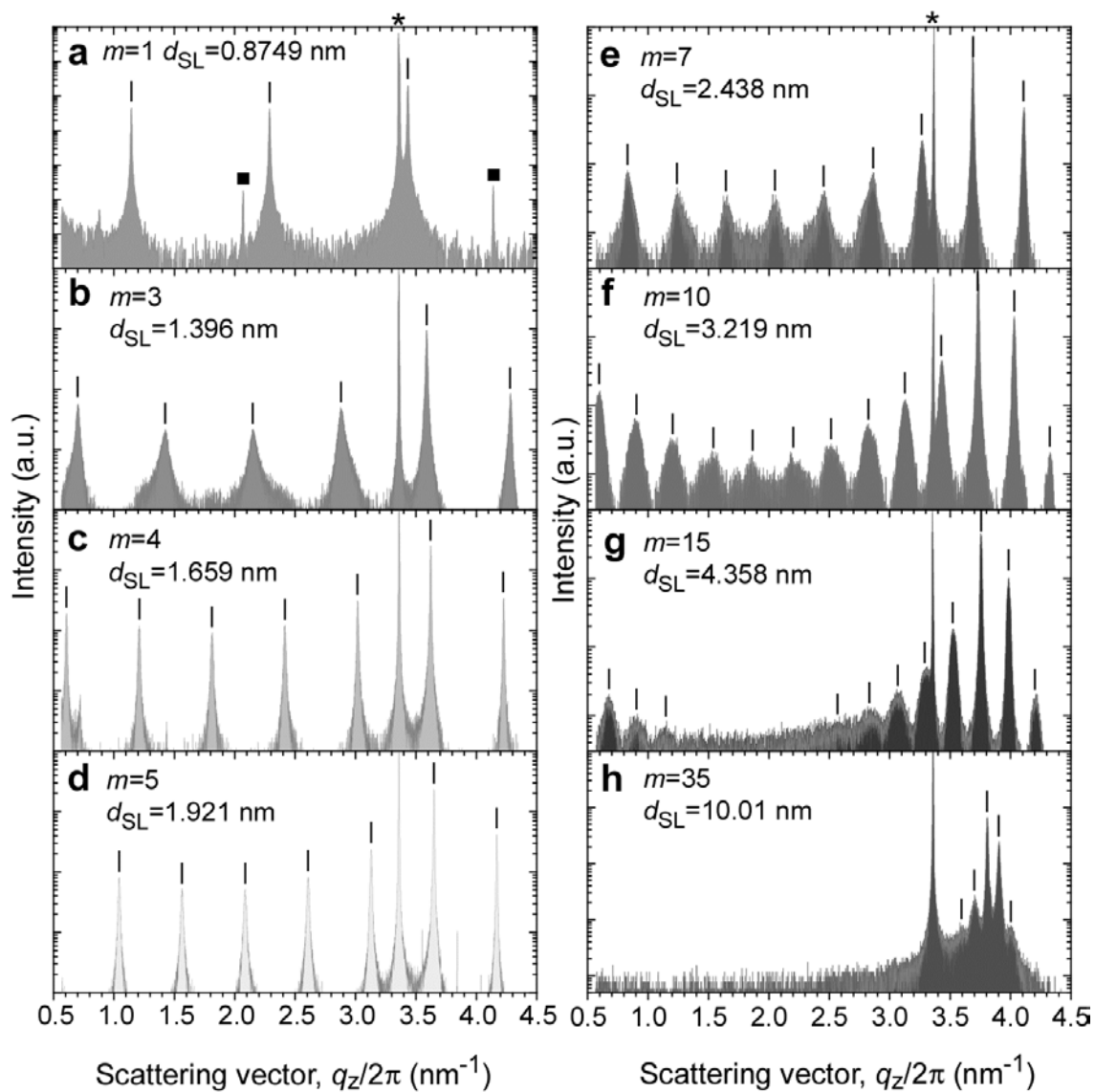
**Figure S2.** Out-of-plane XRD patterns of the resultant InGaO$_3$(ZnO)$_m$ films grown on (111)-oriented YSZ substrates. $m$-values are (a) 1, (b) 3, (c) 4, (d) 5, (e) 7, (f) 10, (g) 15, and (h) 35. Intense diffraction peaks of 000$l$ InGaO$_3$(ZnO)$_m$ ( | ) are seen together with 111 YSZ substrate (*) though tiny amount of the impurity phase was detected (■) in (a).
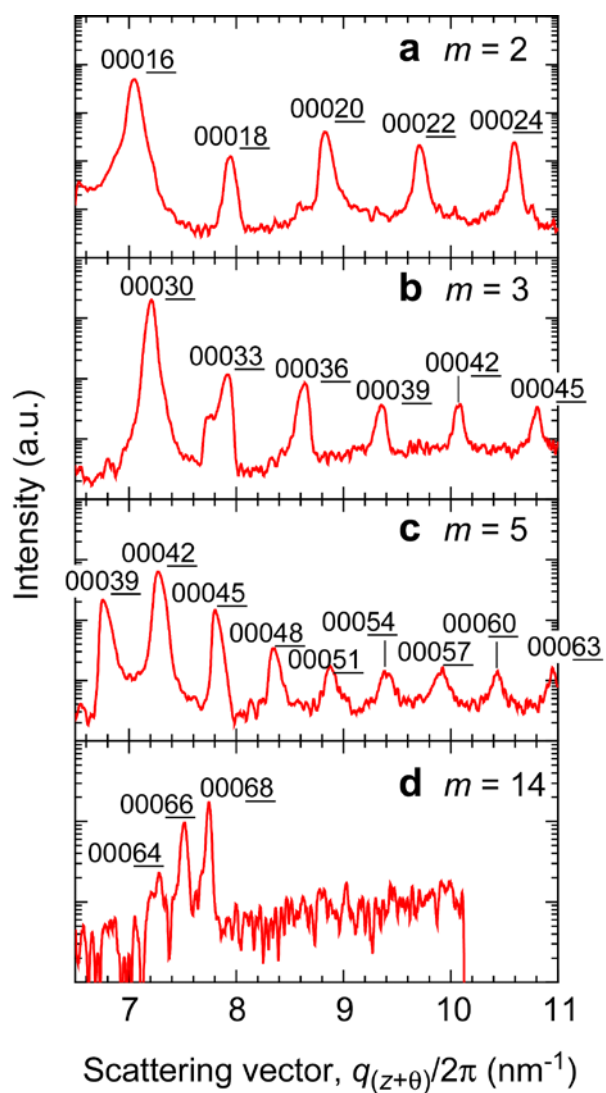
**Figure S3.** Off-axis XRD patterns of the resultant InGaO$_3$(ZnO)$_m$ films grown on (110)-oriented YSZ substrates. *m*-values are (a) 2, (b) 3, (c) 5, and (d) 14. Intense diffraction peaks of 000*l* InGaO$_3$(ZnO)$_m$ are seen when $\theta$ is 31.5°.

InGaO$_3$(ZnO)$_m$ films on (111) YSZ substrates

| $m = 3$ | $m = 5$ | $m = 7$ | $m = 15$ |



500 nm
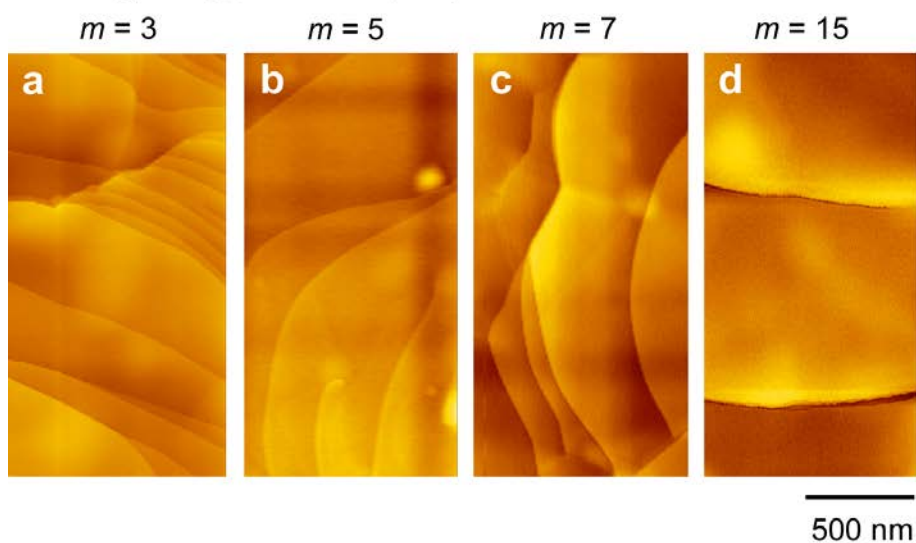
InGaO$_3$(ZnO)$_m$ films on (110) YSZ substrates

| $m = 2$ | $m = 3$ | $m = 5$ | $m = 14$ |



500 nm
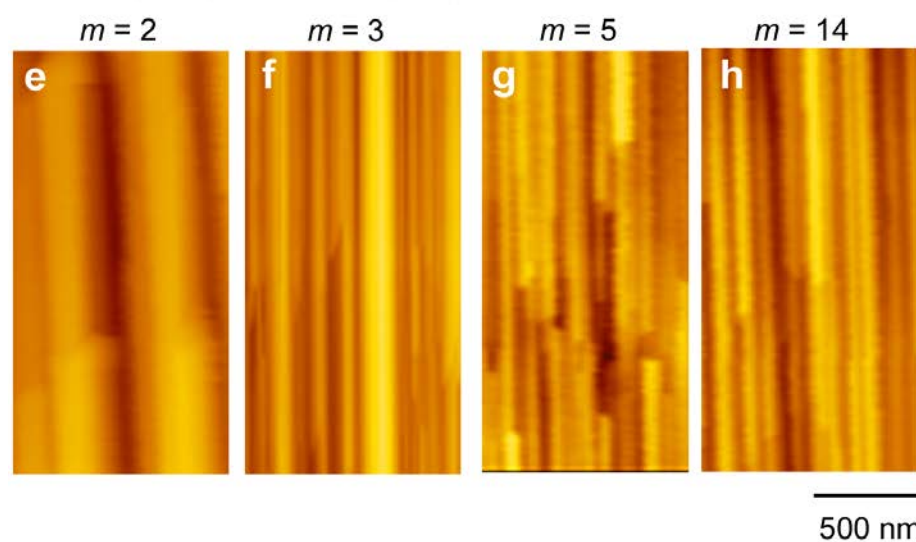
**Figure S4.** Topographic AFM images of the InGaO$_3$(ZnO)$_m$ superlattice films. (a−d) InGaO$_3$(ZnO)$_m$ films grown on (111)-oriented YSZ substrate. $m$-values are (a) 3, (b) 5, (c) 7, and (d) 15 (1 μm × 2 μm). Atomically flat terraces and steps are seen in all cases. e−h, InGaO$_3$(ZnO)$_m$ films grown on (110)-oriented YSZ substrate. $m$-values are (e) 2, (f) 3, (g) 5, and (h) 14 (1 μm × 2 μm). Stripe patterns are seen in all cases.

**References**

[1]     S. H. Firoz, T. Yagi, N. Taketoshi, K. Ishikawa, T. Baba, *Meas. Sci. Technol.* **2011**, *22*, 024012.

[2]     E. H. P. Cordfunke, E. F. Westrum, *J. Phys. Chem. Solids* **1992**, *53*, 361-365.

[3]     S. I. Stepanov, V. I. Nikolaev, V. E. Bougrov, A. E. Romanov, *Rev. Adv. Mater. Sci.* **2016**, *44*, 63-86.

[4]     R. A. Robie, H. T. Haselton, B. S. Hemingway, *J. Chem. Thermodyn.* **1989**, *21*, 743-749.

[5]     M. Nakamura, N. Kimizuka, T. Mohri, M. Isobe, *J. Alloy. Compd.* **1993**, *192*, 105-107.

[6]     M. Nakamura, N. Kimizuka, T. Mohri, *J. Solid State Chem.* **1991**, *93*, 298-315.